ACS APPLIED NANO MATERIALS

www.acsanm.org Article

Copper-Coated Reduced Graphene Oxide Fiber Mesh-Polymer Composite Films for Electromagnetic Interference Shielding

Mingxin Li, Kun Yang, Weiguang Zhu, Junhua Shen, John Rollinson, Mona Hella, and Jie Lian*

Cite This: https://dx.doi.org/10.1021/acsanm.0c00843 Read Online

ACCESS | Metrics & More | Article Recommendations | Supporting Information

ABSTRACT: Expected to become mainstream in the electronics industry, flexible electronics still face major challenging issues. For polymeric-based flexible electronic substrates in particular, these challenges include a lack of electromagnetic shielding capability and poor heat dissipation. Here, we report a highly flexible and thermally conductive macroscopic polydimethylsiloxane (PDMS) polymer film embedded with a copper-coated reduced graphene oxide (rGO) fiber mesh. The rGO fibers are assembled into 3D fiber meshes and electroplated with micrometer-thick copper coatings, displaying excellent electrical and thermal conductivities. Oriented in the horizontal and perpendicular directions within the PDMS polymeric matrix, the fiber mesh serves as a highly electrically and thermally conductive backbone through the in-plane direction. Meanwhile, the fiber mesh also effectively shields electromagnetic interference in the X-band without causing thermal damage. The macroscopic film remains electrically insulated in the through-plane direction. Utilizing both the favorable thermal and electrical properties of the graphene fiber-based mesh and the flexibility of the PDMS matrix, our film may exhibit potential for flexible electronics applications such as wearable electronic thermal management and flexible microwave identification devices.

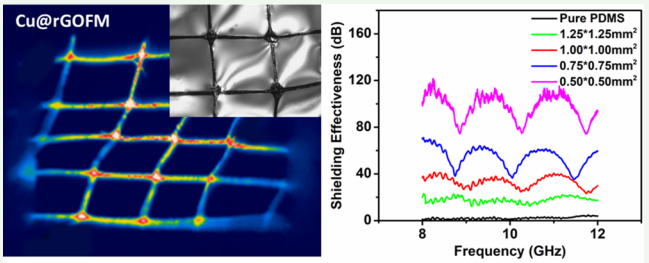

KEYWORDS: *reduced graphene oxide, flexible, fiber mesh, composite film, electromagnetic shielding*

INTRODUCTION

Recently, flexible electronics has generated enormous interest with immense potential for innovation, uprooting conventional silicon-based electronics and changing their designs. However, to outperform the power and efficiency of conventional integrated circuits, flexible electronics will need to achieve the same level of compactness as conventional counterparts. Currently, the major limiting factors to the design, application, and downsizing of flexible electronics include (1) isolation against electromagnetic interference (EMI), electrical leakage, and impacts of moisture,[1,2] and (2) integration of more power consuming components into compact spaces while maintaining acceptable heat dissipation.[3,4] To meet these requirements, multiple metallic and polymeric layers are often employed for packaging conventional electronics.[5,6] EMI shielding and heat management, in particular, often rely on brittle metallic layers,[7,8] which may not be very suitable for flexible electronics.

To better adapt to the functional necessities of packaging flexible electronics into a dense structure, EMI shielding materials based on carbon nanomaterials and flexible polymer matrices have been extensively studied within the past decade.[9−12] Reduced graphene oxide (rGO) has been the graphene-based nanomaterial of choice due to its lightweight, impressive electrical conductivity and ability to form a homogeneous dispersion in various polymer matrices. rGO dispersions upon interaction with ferric ions in a polymer matrix exhibit substantial interfacial polarization and electron mobility, greatly improving microwave absorption capabilities.[13] An added benefit for incorporating rGO into the polymer matrix is higher thermal conductivity. The thermal conductivity enhancement rate can be as high as 357.8% when rGO is covalently bonded to the polymer matrix.[14] However, a large filler concentration is required to break the percolation threshold and form an electrically conductive network. This will often increase material costs and induce other limitations, including trouble forming a homogeneous structure with uniform dispersion of carbonaceous materials.[15] Recently, self-assembled rGO based 3D macroscopic structures have been incorporated into flexible electromagnetic interference shielding composites to increase electrical conductivity and provide mechanical reinforcement.[16] However, through-plane electrical insulation is a significant challenge for such electromagnetic shielding composites as their percolation networks are formed in three dimensions, often leading to power dissipation between adjacent components and even causing short circuits.

Received: March 28, 2020
Accepted: May 19, 2020
Published: May 20, 2020

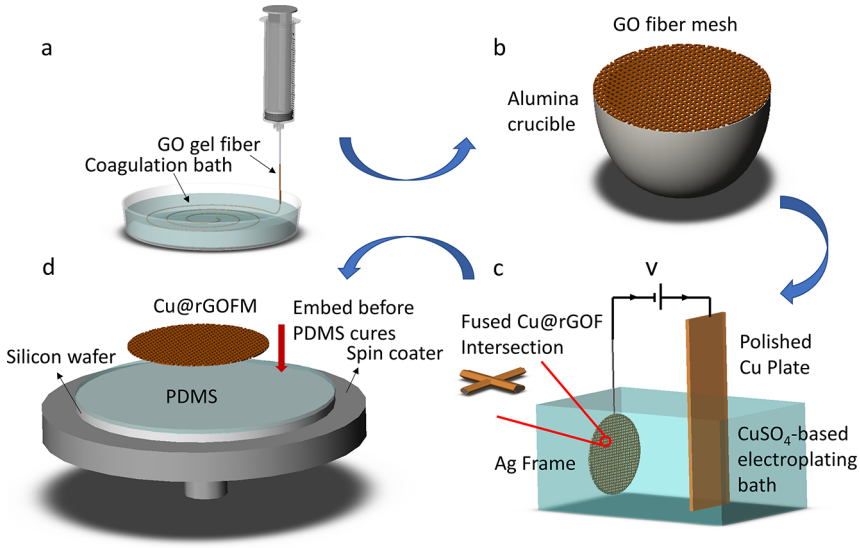

Figure 1. A schematic illustration of the fabrication process of copper-coated reduced graphene oxide fiber mesh and integration into a PDMS matrix. (a) Graphene oxide fibers prepared by wet-spinning. (b) Graphene oxide fiber laid out across an alumina crucible to form a graphene oxide fiber mesh. (c) After the processes of drying, chemical reduction, and thermal annealing, the fiber mesh is removed from the crucible and electroplated in a $CuSO_4$ based bath. (d) Cu@rGOFM is embedded into a spin-coated PDMS matrix before it is cured.

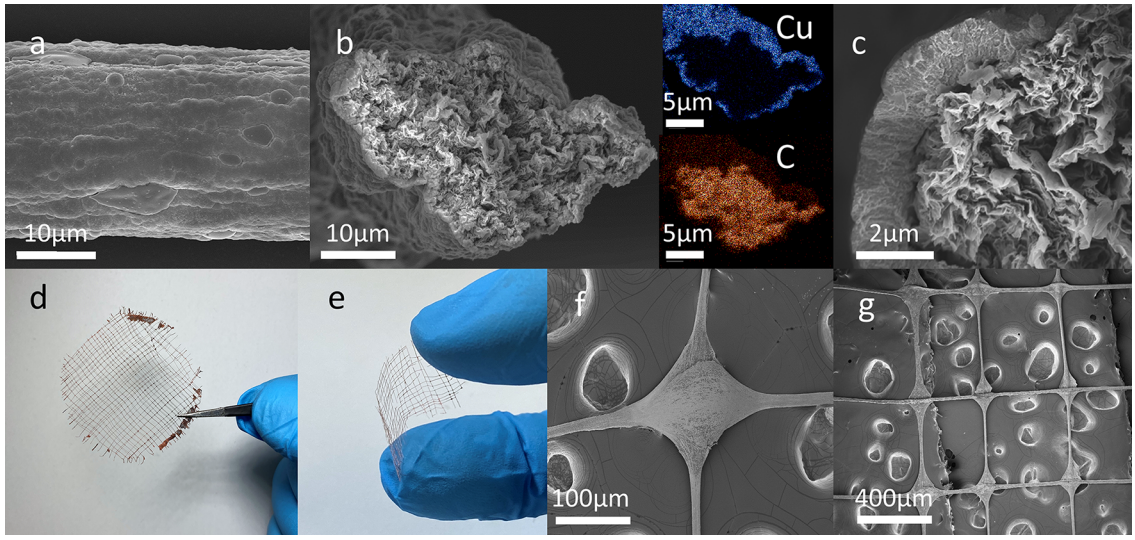

Figure 2. Morphology and microstructure of copper-coated rGO fibers and fiber meshes. (a) SEM image showing morphology of a Cu@rGOF. (b) Cross-sectional SEM image of a Cu@rGOF and elemental mapping. (c) Uniform copper layer coated on a rGO fiber. (d) A 1000 μm × 1000 μm aperture Cu@rGOFM. (e) Flexibility of Cu@rGOFM. (f) Cu@rGOFs fused together at an intersection point within a Cu@rGOFM. (g) Cu@rGOFM SEM image.

This poses difficulties for their direct application in the packaging of flexible electronics.

Two-dimensional graphene oxide (GO) sheets can be assembled into macroscopic fibers through a wet spinning approach. During this process, a shear flow shapes GO lyotropic liquid crystals into fibrous precursors. A highly compact structure can be obtained by subsequent chemical reduction and high temperature thermal annealing of the precursor fibers. High quality graphene fibers display excellent thermal conductivity (1260 $W \cdot m^{-1} \cdot K^{-1}$) and high tensile strength (2.3 GPa).[17,18] By annealing at a milder temperature (~1000 °C), rGO fibers are obtained. Comparing to high quality graphene fibers, the manufacturing of rGO fibers is less energy intensive and easier to be implemented from 2D to 3D materials. Chemical doping, for example, by iodine has been reported to increase the electrical conductivity of rGO fibers from 10^5 up to 2.25×10^7 $S \cdot m^{-1}$.[19] Another advantage of rGO fibers is that their stiffness as represented by Young's modulus can be adjusted in a large range by adding a chemical treatment procedure prior to thermal annealing or fine-tuning thermal annealing time and temperature.[20]

Lightweight, high thermal conductivity, tunable electrical and mechanical properties, and the ease of manufacturing make rGO fibers a promising material for flexible electronics. In this work, we demonstrate the potential of integrating highly flexible and conductive rGO fibers into a polymer matrix to form a 3D macroscopic structure that could be useful for packaging and electromagnetic interference (EMI) shielding applications in flexible electronics. The wet spun GO fibers are closely laid out in a 2D mesh configuration as in conventional

https://dx.doi.org/10.1021/acsanm.0c00843
ACS Appl. Nano Mater. XXXX, XXX, XXX−XXX

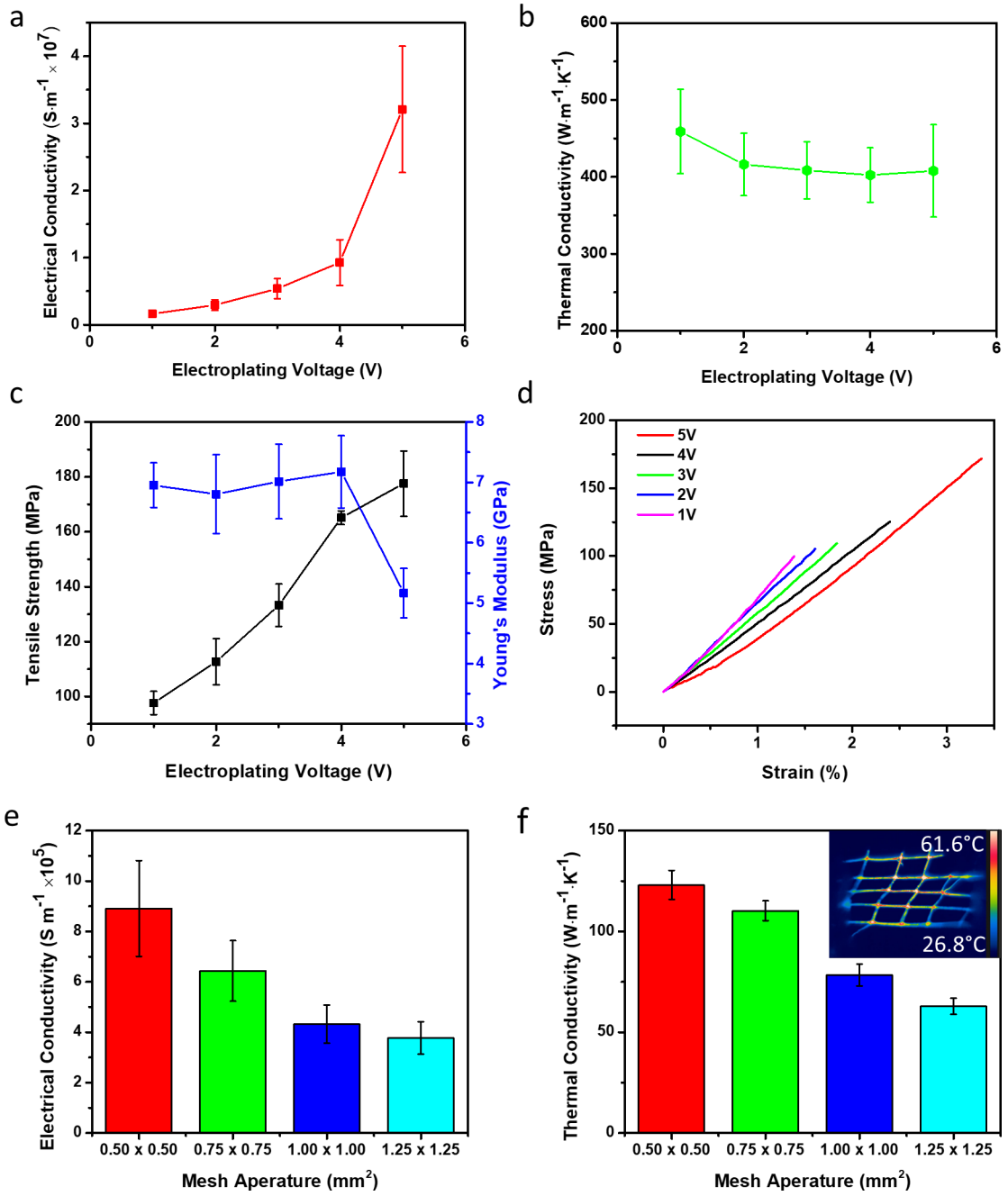

Figure 3. Electrical, thermal, and tensile properties of copper coated rGO fibers and fiber meshes. (a) Electrical conductivity of Cu@rGOFs. (b) Thermal conductivity of Cu@rGOFs. (c) Tensile strength and Young's modulus of Cu@rGOFs. (d) Stress−strain curves of Cu@rGOFs. (e) Electrical conductivity of Cu@rGOFMs (Cu coating thickness ∼4.5 μm). (f) Thermal conductivity of Cu@rGOFMs (Cu coating thickness ∼4.5 μm) (inset: an infrared image of a Cu@rGOFM during thermal conductivity measurement).

EMI shielding metal wired meshes. The GO fiber meshes are dried, chemically reduced, and thermally annealed at mild temperatures. Individual fibers that form the mesh are fused together at intersections giving the mesh a high thermal conductivity and good integrity. A thin uniform coating of copper is electroplated onto the mesh for exemplary electrical conductivity. PDMS is chosen as the film substrate to embed the copper-coated rGO fiber mesh (Cu@rGOFM) due to its flexibility and electrical insulating property.[21−23] The architecture of this 3D mesh-polymer composite structure allows for excellent in-plane electrical and thermal conductivities, ensuring superb EMI shielding capability while the PDMS matrix electronically insulates the film in the through-plane direction.

RESULTS AND DISCUSSION

Figure 1 illustrates the fabrication process of the copper-coated rGO fiber mesh and its integration into a PDMS matrix in order to design excellent EMI shielding materials with the capability of resisting overheating and providing sufficient through-plane electrical insulation. In EMI shielding materials, a highly electrically conductive percolation path perpendicular to the transmission direction of the electromagnetic wave is a key to increasing shielding effectiveness. After the wet-spinning

https://dx.doi.org/10.1021/acsanm.0c00843
ACS Appl. Nano Mater. XXXX, XXX, XXX−XXX

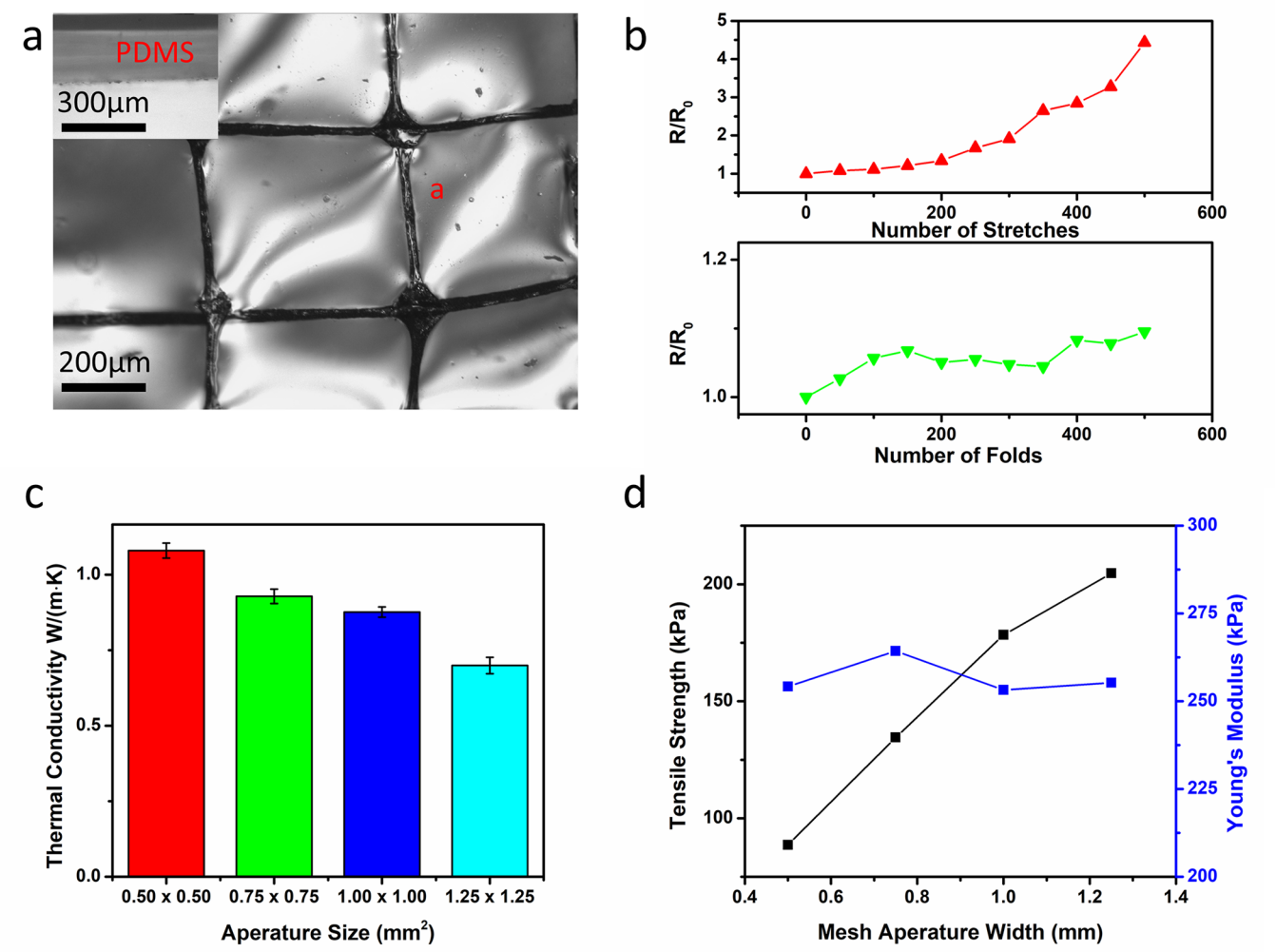

Figure 4. A copper-coated rGO fiber mesh embedded PDMS composite film and their properties. (a) An optical image showing morphology of the Cu@rGOFM embedded PDMS composite film (*a*, aperture width) (inset figure, cross-section of PDMS film). (b) Electrical resistance variation after stretching and folding. (c) Thermal conductivity of the Cu@rGOFM (Cu coating thickness ~4.5 μm) embedded PDMS composite films. (d) Tensile strength and Young's modulus of the Cu@rGOFM embedded PDMS composite films.

process, the GO-gel fibers are suspended in a 90° grid pattern. Followed by drying, chemical reduction, and thermal annealing at 1000 °C for 2 h, the GO-gel fibers are fused together into an interconnected mesh. The resulting rGO fiber mesh is electroplated in a $CuSO_4$ based solution at a constant voltage for 20 s. Figure 2 presents the morphology and microstructure of the graphene fiber mesh showing a uniform copper coating on the surface of rGO fibers. The thickness of the copper coating can be precisely controlled to ~0.5 μm (Figure 2b). This thin coating of copper ensures excellent electrical conductivity of the embedded network while retaining the flexibility and lightweight of low temperature-annealed rGO fibers (Figure 2d,e). The chemical composition and crystalline structure of the pristine rGO fiber mesh (rGOFM) and the Cu@rGOFM are investigated using Raman spectroscopy and X-ray diffraction (XRD), respectively. Raman spectral peaks of rGO at ~1580 cm^{-1} (G band) and ~2700 cm^{-1} (2D band) are identified for rGOFM.[20,24,25] The absence of both G band peak and 2D band peak in the Cu@rGOFM Raman spectrum along with a clear copper fluorescence background demonstrates the conformity of the copper coating (Figure S1a). An XRD spectrum (Figure S1b) of the Cu@rGOFM shows diffraction peaks of Cu (111), (200), (220) at 43.6°, 50.7° and 74.4° respectively,[26−28] suggesting a polycrystalline nature of the copper coatings without the formation of copper oxides.

The microstructure, electrical, thermal, and mechanical properties of the copper-coated rGO fibers (Cu@rGOFs) can be optimized by carefully controlling thermal treatment conditions and tuning electroplating voltages (see Figure 3a−c). The electrical conductivity of the Cu@rGOFs is governed by the average thickness of the electroplated copper coating. As the coating increases from 0.62 to 4.69 μm (Figure S3) at higher electroplating potentials, the electrical conductivity of the Cu@rGOFs increases from 1.6×10^6 to 3.2×10^7 $S{\cdot}m^{-1}$ (Figure 3a). The Cu@rGOFs have a high conductivity to weight ratio (1.23×10^4 $S{\cdot}m^2{\cdot}kg^{-1}$) on par to that of commercially available copper wire (3.15×10^4 $S{\cdot}m^2{\cdot}kg^{-1}$) due to its low density (2.59 $g{\cdot}cm^{-3}$ for Cu@rGOFs electroplated at 5 V).

In addition to impressive electrical conductivities at room temperatures, the Cu@rGOFs are also resilient against resistivity increase due to heat accumulation (Figure S4c). This is a result of a high thermal conductivity (461.2 $W{\cdot}m^{-1}{\cdot}K^{-1}$) for pristine rGOF. Therefore, any Joule heat generated on the copper coating of the Cu@rGOFs can be easily conducted away through the rGOF core. As the electroplating voltage

https://dx.doi.org/10.1021/acsanm.0c00843
ACS Appl. Nano Mater. XXXX, XXX, XXX−XXX

increases to 5 V, dendritic formation of copper crystals occurs on the fiber surface (Figure S3e). These dendrites not only increase the ratio of copper to rGO in the fiber cross-section but also significantly increases the surface area of the Cu@rGOF. This can further dissipate Joule heat and prevent heat-induced resistivity increase.[29] Similar dendrite formations also occurred during previous attempts of electroplating thin metal coatings onto graphene-based materials.[26] However, these dendrites usually indicate weak bonding between the graphene (or rGO) and metal interface, detrimental to the fiber's inherent mechanical properties and the interfacial strength between it and the PDMS matrix. Hence, fibers electroplated at voltages of higher than 5 V are not further studied.

By limiting heating rates to 1 °C·min^{-1} and extending thermal annealing time to 2 h, the residue oxygen-containing functional groups within the fibers are mostly depleted through a slow outgassing process,[30] decreasing phonon scattering within the fibers. This results in outstanding thermal conductivity of the rGOFs. When electroplated at a low potential of 1 V, the thickness of the copper layer is insignificant. Heat conduction occurs overwhelmingly through the rGO core and the thermal conductivity of the Cu@rGOF reaches a high value of 459.0 W·m^{-1}·K^{-1} (Figure 3b). As the copper layer thickness increases, thermal conductivities of Cu@rGOFs decrease due to copper having a lower thermal conductivity than rGOF.

On the other hand, the removal of oxygen containing cross-links (Figure S1c) will result in fibers with lesser cross-links and a lower tensile strength.[19] In the Cu@rGOFs' case, the oxygen functional groups of the rGO core have been substantially outgassed to increase thermal conductivity, reducing its tensile strength. However, while reducing thermal transport, copper coating contributes more to the tensile strength of the fibers than the rGO core. Therefore, increasing electroplating potential enhances mechanical properties of the fiber. The highest tensile strength can be found when the fiber is electroplated at 5 V as shown in Figure 3c,d. The Young's modulus of the Cu@rGOFMs remains relatively unchanged with the electroplating potential varying from 1 to 4 V. Therefore, careful controlling of thermal annealing and electroplating is required to balance the desired thermal and electrical conductivities and mechanical properties of the coated fibers.

A synergetic positive effect of Cu coating on the electrical and thermal conductivities can also be observed on Cu@rGOFMs. Figure 3e shows the electrical conductivity of the 500 μm × 500 μm Cu@rGOFM electroplated at 5 V reaching a high of 8.90 × 10^5 S·m^{-1}. This represents 68 times greater than that of the 500 μm × 500 μm rGOFM (1.30 × 10^4 S·m^{-1}) without copper coating, outperforming both graphene paper and the latest graphene-based fabrics.[31,32] Figure 3f also shows that its thermal conductivity is on par with that of pristine graphene papers. rGOFMs significantly reduces the consumption of the graphene oxide precursors as compared to graphene papers.[31]

On one hand, the high in-plane electrical and thermal conductivities of the Cu@rGOFM are essential to meeting the needs for electromagnetic shielding and heat dissipation in flexible electronics. On the other hand, the electrical percolation in the through-plane direction may lead to power dissipation and even short circuits between individually package components. Thus, reliable through-plane electrical insulation is necessary for enabling its application in flexible electronics. To achieve this, the Cu@rGOFM is fully embedded into a PDMS film approximately 150 μm thick (Figure 4a). This polymer matrix provides flexibility for the network within the film while achieving electrical insulation in the through-plane direction. Surface resistance of the film is measured to be 1.28 × 10^5 Ω·m for composite films embedded with a 500 μm × 500 μm Cu@rGOFM, suggesting effective insulation in the through-plane direction.

Cyclic strain and folding are performed on Cu@rGOFMs to test the in-plane electrical conductivity response of the composite film. The resistance change of PDMS films embedded with the 500 μm × 500 μm Cu@rGOFM is studied using a motorized stage providing 50% cyclic strains. As shown in Figure 4b, the resistance of the composite film increases slowly when the stretching cycle is under 200. During this time, even though fractures occur at the intersection points of the Cu@rGOFM, the highly elastic PDMS matrix will bring the fractured surfaces back into contact when the strain is released. After more than 200 cycles of stretching, small fractures occurring within the PDMS matrix increases the film resistance. As compared to stretching, the Cu@rGOFM behaves in a more flexible manner during folding (as shown in Figure 2e). This explains the low resistance increase of the composite film even after 500 cycles of folding.

The thermal conductivity of PDMS composite films embedded with Cu@rGOFMs of various aperture sizes are obtained through laser flash analysis. Though two magnitudes lower than that of standalone Cu@rGOFMs, the reported value of the composite (as shown Figure 4c) is still about 10 times greater than neat PDMS films.[33] This is impressive considering the highest volumetric ratio of the Cu@rGOF in the composite film is below 1%. In comparison, the highest reported thermal conductivity of a rGO/PDMS composite at a similarly low loading is only 0.68 W·m^{-1}·K^{-1},[34] about 50% lower than that of the Cu@rGOFM reported here. Further increasing the thermal conductivity of the composite film can be achieved by decreasing the film thickness or fiber mesh aperture or embedding multiple layers of Cu@rGOFM. However, decreasing the mesh aperture width below 500 μm in order to further increase thermal conductivity will reduce the tensile strength of the composite film. Figure 4d also shows that within the range of 500−1250 μm aperture width does not affect the Young's modulus of the composite film. The tensile strength and Young's modulus of the composite films from the tensile testing are supported by the simulation results derived from the Zweben−Rosen uniaxial tensile model and Halpin−Tsai model.[35−37] The simulation and its results are discussed in detail in the Supporting Information (Figure S6).

The electromagnetic interference shielding effectiveness (EMI SE) of a pure PDMS film and the Cu@rGOFM embedded PDMS films are measured in the X-band (8−12 GHz). The EMI SE of the pure polymeric film is measured as 2.2 dB. The EMI SE of the 1250 μm × 1250 μm Cu@rGOFM embedded PDMS film at the same thickness remains consistently above 23.3 dB across the entire frequency range of the X-band, above the requirement of EMI SE of 20 dB for laptops and other common electrical appliances. The high-frequency dependence and the fluctuation of the EMI SE in the form of a standing wave can be contributed to the interference of the X-band microwave within the Fabry−Perot chamber-like enclosure formed in between the waveguide adapters and the copper coating of the Cu@rGOFM.[38] In general, the Fabry−Perot interference is more pronounced for

https://dx.doi.org/10.1021/acsanm.0c00843
ACS Appl. Nano Mater. XXXX, XXX, XXX−XXX

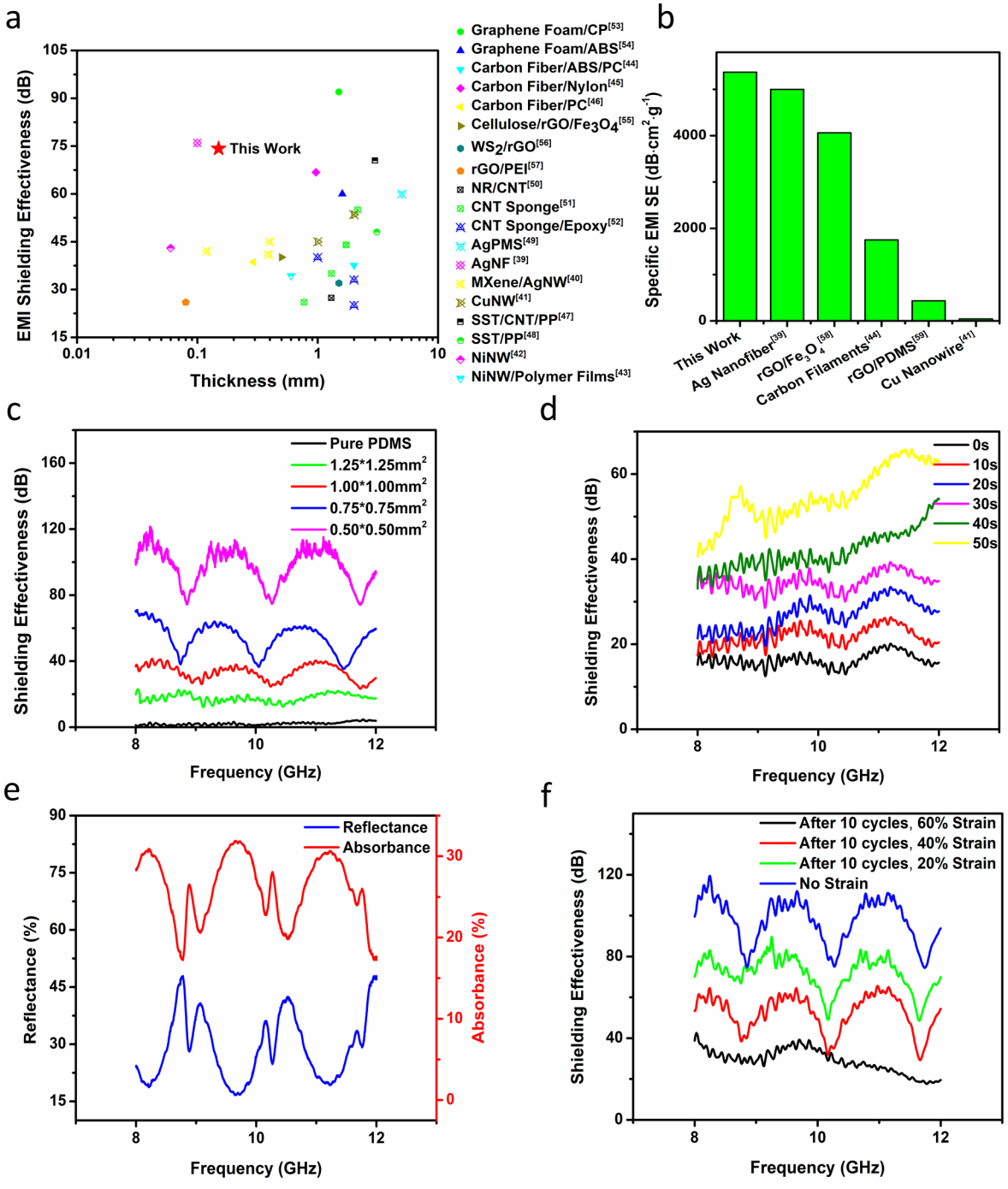

Figure 5. Electromagnetic interference shielding effectiveness properties of copper-coated reduced graphene oxide fiber mesh embedded PDMS composite films. (a) Comparison of thickness and maximum EMI SE of the Cu@rGOFM embedded PDMS composite films with of the state-of-the-art materials reported recently. (b) Comparison of specific EMI SE of the Cu@rGOFM embedded PDMS composite film with relevant materials. (c) EMI SE measurements of the composite films with Cu@rGOFMs (copper coating thickness ~4.5 μm) of various apertures. (d) EMI SE measurements of the composite films with Cu@rGOFMs of various electroplating time. (e) Reflection and absorption rates of electromagnetic waves by composite film embedded with 500 μm × 500 μm Cu@rGOFM. (f) EMI SE measurements of the composite films embedded with 500 μm × 500 μm Cu@rGOFMs (copper coating thickness ~4.5 μm) after cycling 10 times at various strain rates.

the films embedded with Cu@rGOFM of smaller apertures due to more microwave reflections between the waveguide adapters and the copper coating of the Cu@rGOFM. Despite the convolution of the EMI SE contribution of the Cu@rGOFM embedded PDMS films with the Fabry−Perot interference, it is sufficient to claim that the EMI SE after devolution for the samples with the 500 μm × 500 μm aperture should still be consistently above 74.2 dB. This is because the lowest convoluted EMI SE value 74.2 dB corresponds to the attenuation phase of the Fabry−Perot interference. We further compare the EMI SE of the composite film with the state-of-the-art materials. As shown in Figure 5a, the EMI SE of our composite film is among the top tier of EMI shielding materials reported in recent literature, including silver

https://dx.doi.org/10.1021/acsanm.0c00843
ACS Appl. Nano Mater. XXXX, XXX, XXX−XXX

nanowires,[39,40] copper nanowires,[41] nickel fibers,[42,43] carbon fibers,[44−46] stainless steel fibers,[47,48] silver sponges,[49] CNT sponges,[50−52] graphene foams,[53,54] and rGO nanocomposites.[55−57] With a physical density of 0.921 g·cm^{-3}, the specific EMI SE of the composite film reaches to 5371.0 dB·g·cm^{-2}, which is equally impressive compared to its peers (Figure 5b).[39,41,44,58,59]

The shielding effectiveness of the composite films can be controlled with different mesh designs and electroplating durations. Specifically, EMI SE decreases with an increased mesh aperture size (Figure 5c) and increases proportionally at longer electroplating times (Figure 5d). An increase in electroplating time does not increase Fabry−Perot interference. Figure 5d shows the EMI SE of the composite films (embedded with 1250 μm × 1250 μm Cu@rGOFM) electroplated at different durations. Despite increased copper coating thickness at longer electroplating times, the volumetric ratio of copper in the 1250 μm × 1250 μm Cu@rGOFM is still lower than that of a 500 μm × 500 μm Cu@rGOFM. This translates to less microwave reflection between the waveguide adapters and the copper coating of the embedded 1250 μm × 1250 μm Cu@rGOFM. For composite films with smaller mesh apertures, a more uniform EMI SE can be achieved across the X-band by increasing electroplating time. On the other hand, the copper coating thickness increases with electroplating time, and density of the embedded Cu@rGOFM will correspondingly increase, while its thermal conductivity will decrease.

The underlying EMI shielding mechanism of the composite film is further studied through the analysis of complex scattering parameters acquired from a two-port vector network analyzer (VNA). The incoming through-plane EM wave partly transmits through and partly gets absorbed and reflected by the composite film. In accordance with other previously reported graphene-based EMI shielding materials,[60−62] absorption in the X-band is the dominate effect of the Cu@rGOFM embedded PDMS composite films on through-plane electromagnetic waves (Figure 5e). Reflection of the electromagnetic waves off from the thin copper coating of the Cu@rGOFM is the secondary effect. Though absorption results in the energy of the EM waves being transformed into heat, heat accumulation is not an issue for the Cu@rGOFM embedded PDMS composite film. The generated heat can be readily dissipated through the highly thermally conductive rGO core, preventing the Cu@rGOFM embedded PDMS composite films from overheating during the EMI shielding process. Tested in the X-band range, the highest temperature rise within the composite film after 1 min is 1.2 °C.

The resistance of the EMI SE properties of the Cu@rGOFM embedded PDMS to mechanical deterioration is further studied by subjecting the film to cyclic tensile strain prior to EMI SE measurement (Figure 5f). Despite some degradation of film integrity, after 10 cycles at the strain rate of 40%, the average EMI SE of the relaxed 500 μm × 500 μm aperture film can still reach 52.4 dB (29.2 dB at the lowest). Under strain below 50%, some of the fused connections of the Cu@rGOFMs fractured. However, as previously mentioned, once relaxed, the elasticity of the PDMS matrix brought the fractured surfaces back into contact. This partially restores the percolation path of the Cu@rGOFMs, which is crucial to the good EMI shielding capability of the composite film. Only after cycling at very high strain rates of 60% and above will the EMI SE significantly deteriorate.

CONCLUSIONS

In conclusion, we have demonstrated an innovative and versatile solution to achieve simultaneous electronic insulation packaging and EMI shielding for flexible electronics in the form of Cu@rGOFM embedded PDMS composite films. The horizontally and transversely aligned fibers fuse to each other to form 2D fiber meshes and are coated with a thin copper film through electroplating. As a result of outstanding electrical and thermal conductivities of the Cu@rGOFs (up to 3.21 × 10^7 S·m^{-1} and 459 W·m^{-1}·K^{-1}), respectively, the mesh structure can significantly improve the electrical and thermal conductivities of the composite film. The high electrical conductivity of the fiber mesh renders the composite film excellent EMI SE up to 74.2 dB. The specific EMI SE of the composite film also leads among similar EMI shielding materials. The high thermal conductivity of the rGO fiber helps to remove the localized heating and alleviates Joule heat-induced resistivity increase of the fiber mesh during the EMI shielding process, as evidenced by a low-temperature increase in the composite films exposed to X-band microwaves. The PDMS matrix provides an excellent electrical insulation for the film in the through-plane direction. Due to their lightweight, flexible, electrically, and thermally conductive nature, the Cu@rGOFM embedded PDMS composite films may possess potentials for a wide range of applications in the field of flexible electronics.

EXPERIMENTAL SECTION

Materials. Graphite intercalation compounds (99.99%, 50 mesh) were purchased from Qingdao Nanshu Graphite Co. Ltd. Copper(II) sulfate pentahydrate ($CuSO_4·5H_2O$) (98%), hexadecyltrimethylammonium bromide (99%), and polyethylene glycol (avg. M_v 4000) were purchased from Sigma-Aldrich. NaCl (95%), H_2SO_4 (98%), ethyl acetate, tetrabromoethane ($Br_2CHCHBr_2$), carbon tetrachloride (CCl_4), and *N*,*N*-dimethylformamide (DMF) (99.8%) were purchased from Fisher Chemical. Polydimethylsiloxane (PDMS) precursors were purchased from Dow Chemical Company.

rGO Fiber Mesh Fabrication. Graphene oxide (GO) was prepared from graphite powders using a modified Hummer's method.[31,63] The GO gel was wet spun using 23 gauge syringe dispensing needles into a coagulation bath with a ethyl acetate to DMF volumetric ratio of 2:1. After immersing in the coagulation bath for 10 min, the GO gel fibers were snipped into short pieces and laid parallel to each other across the rim of an alumina crucible. The fibers were dried for 2 h, before another group of freshly coagulated GO gel fibers were laid perpendicularly on top of them. The GO gel fibers on top that were still wet moisturized the dried fibers that they were laid upon, forming intersections between fibers perpendicular to each other. The fiber meshes were then dried for 2 h, chemically reduced using hydroiodic acid (HI) for 24 h at 90 °C and thermally annealed at 1000 °C for 2 h in a tube furnace. The heating rate for the tube furnace was set at 1 °C·min^{-1}. The GO fiber meshes were kept on an alumina crucible throughout the chemical reduction and thermal annealing processes and an axial tension was applied on the fibers of the mesh to prevent shrinkage.

Electroplating Process. The electroplating was conducted on a VersaSTAT 4 electrochemical workstation. The thermally annealed rGO mesh was lifted from the alumina crucible and pasted to a silver wire frame with conductive silver paste. The silver frame held rGO mesh was used as a cathode after the silver paste dried, and a polished copper plate was used as the anode. The electroplating bath was a mixed aqueous solution of $CuSO_4·5H_2O$ (250 g·L^{-1}), H_2SO_4 (3 mL·L^{-1}), NaCl (128.5 mg·L^{-1}), polyethylene glycol (352 mg·L^{-1}), and hexadecyltrimethylammonium bromide (10 mg·L^{-1}).[64] The electroplating bath was deaerated with argon for 30 min before usage. During electroplating, the workstation was set to potential-static, and the rGO meshes were placed in parallel to the copper anode. The

https://dx.doi.org/10.1021/acsanm.0c00843
ACS Appl. Nano Mater. XXXX, XXX, XXX−XXX

rGO meshes were electroplated for 10 s on each side. After electroplating, the meshes were carefully dipped into DI water to rinse any residue before drying.

Characterization. The morphology and microstructure of the fibers were characterized by a field-emission scanning electron microscope (SEM) Carl Zeiss Supra 55. Energy-dispersive X-ray spectroscopy was conducted on the cross-section of individual fibers using Oxford INCA EDS. Raman spectroscopy was performed with a LabRAM HR800 Raman microscope using a 532.18 nm green laser light source and 600 g·mm^{-1} grating. X-ray diffraction (XRD) patterns were collected with a PAN analytical X-ray diffraction system at a scanning speed of 4° min^{-1}.

The electrical conductivity of the Cu@rGOFM was analyzed by measuring the current and voltage across an individual Cu@rGOF suspended in between two isolate Cu struts using a Fisherbrand digital autorange multimeter. Thermal conductivity of the fibers and mesh were measured using an electrical self-heating approach in which the same setup for electrical conductivity was enclosed into a vacuum chamber with a ZnSe infrared viewport at 10^{-3} Torr. The temperature profile of the fiber was obtained with a FLIR A325sc infrared camera for thermal conductivity measurements.

The density of the mesh samples was measured by the sink-float method during which tetrabromoethane ($Br_2CHCHBr_2$) and carbon tetrachloride (CCl_4) were used.[20] Tensile strength of the Cu@rGOFs were tested using an Instron 5843 electro-mechanical test system with 0.5 mm·min^{-1} extension rate. The surface resistivity of the PDMS embedded mesh was measured with a Suss Manual 4 probe station.

EMI Shielding Measurements. The experimental setup for measuring EMI shielding effectiveness of the Cu@rGOFM embedded PDMS films is shown in Figure S7. A vector network analyzer (Anritsu MS4647B) was used to obtain the scattering parameters (S_{11} and S_{21}) in the X-band frequency (8−12 GHz). S_{11} and S_{12} are correlated to reflectance (R), transmittance (T), and absorbance (A), respectively, according to the following equations[65−67]

$$R = |S_{11}|^2 \tag{1}$$

$$T = |S_{21}|^2 \tag{2}$$

$$A = 1 - R - T \tag{3}$$

The total EMI shielding effectiveness (SE_{Total}) of the Cu@rGOFM embedded PDMS films consists of three parts, each representing the contribution of reflection (SE_R), absorption (SE_A), and multiple reflections (SE_M). In the case of this study, the sum of SE_R and SE_A are greater than 10 dB, thus the contributions of SE_M are deemed to be negligible.[62,64,68] SE_R and SE_A can be described using R and T using the following equations

$$SE_R = -10 \log(1 - R) \tag{4}$$

$$SE_A = -10 \log\left(\frac{T}{1 - R}\right) \tag{5}$$

Thus, SE_{Total} can be described with the following equation

$$SE_{Total} = SE_R + SE_A \tag{6}$$

■ ASSOCIATED CONTENT

Supporting Information

The Supporting Information is available free of charge at https://pubs.acs.org/doi/10.1021/acsanm.0c00843.

Synthesis of GO gel; thermal conductivity measurement of copper-coated reduced graphene oxide fiber (Cu@rGOF) and copper-coated reduced graphene oxide fiber mesh (Cu@rGOFM); composite film ultimate tensile strength calculation; composite film Young's modulus calculation; Cu@rGOFM embedded PDMS composite film in-plane thermal conductivity measurement (PDF)

■ AUTHOR INFORMATION

Corresponding Author

Jie Lian − *Department of Mechanical, Aerospace, and Nuclear Engineering, Rensselaer Polytechnic Institute, Troy, New York 12180, United States;* orcid.org/0000-0002-9060-8831; Email: lianj@rpi.edu

Authors

Mingxin Li − *Department of Mechanical, Aerospace, and Nuclear Engineering, Rensselaer Polytechnic Institute, Troy, New York 12180, United States;* orcid.org/0000-0003-3276-9140

Kun Yang − *Department of Mechanical, Aerospace, and Nuclear Engineering, Rensselaer Polytechnic Institute, Troy, New York 12180, United States*

Weiguang Zhu − *Department of Mechanical, Aerospace, and Nuclear Engineering, Rensselaer Polytechnic Institute, Troy, New York 12180, United States*

Junhua Shen − *Department of Material Science and Engineering, Rensselaer Polytechnic Institute, Troy, New York 12180, United States*

John Rollinson − *Department of Electrical, Computer, and Systems Engineering, Rensselaer Polytechnic Institute, Troy, New York 12180, United States*

Mona Hella − *Department of Electrical, Computer, and Systems Engineering, Rensselaer Polytechnic Institute, Troy, New York 12180, United States*

Complete contact information is available at: https://pubs.acs.org/10.1021/acsanm.0c00843

Notes

The authors declare no competing financial interest.

■ ACKNOWLEDGMENTS

This work was financially supported by the U.S. National Science Foundation under the award of DMR 1742806.

■ REFERENCES

(1) Rieutort-Louis, W.; Sanz-Robinson, J.; Moy, T.; Liechao, H.; Yingzhe, H.; Afsar, Y.; Sturm, J.; Verma, N.; Wagner, S. Integrating and Interfacing Flexible Electronics in Hybrid Large-Area Systems. *IEEE Trans. Compon., Packag., Manuf. Technol.* **2015**, *5* (9), 1219−1229.

(2) Chen, J.; Huang, X.; Sun, B.; Jiang, P. Highly Thermally Conductive Yet Electrically Insulating Polymer/Boron Nitride Nanosheets Nanocomposite Films for Improved Thermal Management Capability. *ACS Nano* **2019**, *13* (1), 337−345.

(3) Sorrentino, A. Nanocaotings and ultra-thin films for packaging applications. In *Nanocoatings and ultra-thin films; technologies and applications*; Makhlouf, A., Tiginyanu, I., Eds.; Woodhead Publishing: Oxford, 2011; pp 203−234.

(4) Wang, X.; Cui, Y.; Li, T.; Lei, M.; Li, J.; Wei, Z. Recent advances in the functional 2D photonic and optoelectronic devices. *Adv. Opt. Mater.* **2019**, *7* (3), 1801274.

(5) Chao, C.; Scholz, K.; Leibovitz, J.; Cobarruviaz, M.; Chang, C. Multi-layer thin-film substrates for multi-chip packaging. *IEEE Trans. Compon., Hybrids, Manuf. Technol.* **1989**, *12*, 180−184.

(6) Suga, T.; Takahashi, A.; Saijo, K.; Oosawa, S. New fabrication technology of polymer/metal lamination and its application in electronic packaging. *First International IEEE Conference on Polymers and Adhesives in Microelectronics and Photonics. Incorporating POLY, PEP & Adhesives in Electronics. Proceedings* **2001**, 29−34.

(7) Jiang, F.; Li, M.; Gao, L. Research on conformal EMI shielding Cu/Ni layers on package. *2014 15th International Conference on Electronic Packaging Technology* **2014**, 227−230.

(8) Ardebili, H.; Pecht, M. *Encapsulation technologies for electronic applications*; William Andrew: Norwich, NY, 2009.
(9) Jia, L.; Yan, D.; Yang, Y.; Zhou, D.; Cui, C.; Bianco, E.; Lou, J.; Vajtai, R.; Ajayan, P.; Li, Z. High strain tolerant EMI shielding using carbon nanotube network stabilized rubber composite. *Adv. Mater. Technol.* **2017**, *2* (7), 1700078.
(10) Zhao, B.; Zhao, C.; Li, R.; Hamidinejad, S.; Park, C. Flexible, Ultrathin, and High-Efficiency Electromagnetic Shielding Properties of Poly(Vinylidene Fluoride)/Carbon Composite Film. *ACS Appl. Mater. Interfaces* **2017**, *9* (24), 20873−20884.
(11) Zhu, S.; Xing, C.; Wu, F.; Zuo, X.; Zhang, Y.; Yu, C.; Chen, M.; Li, W.; Li, Q.; Liu, L. Cake-like flexible carbon nanotubes/graphene composite prepared via a facile method for high-performance electromagnetic interference shielding. *Carbon* **2019**, *145*, 259−265.
(12) Liang, C.; Hamidinejad, M.; Ma, L.; Wang, Z.; Park, C. Lightweight and flexible graphene/SiC-nanowires/ poly(vinylidene fluoride) composites for electromagnetic interference shielding and thermal management. *Carbon* **2020**, *156*, 58−66.
(13) Singh, A.; Garg, P.; Alam, F.; Singh, K.; Mathur, R.; Tandon, R.; Chandra, A.; Dhawan, S. Phenolic resin-based composite sheets filled with mixtures of reduced graphene oxide, γ-Fe2O3 and carbon fibers for excellent electromagnetic interference shielding in the X-band. *Carbon* **2012**, *50*, 3868−3875.
(14) Li, A.; Zhang, C.; Zhang, Y. Thermal conductivity of graphene-polymer composites: Mechanisms, properties, and applications. *Polymers* **2017**, *9* (12), 437.
(15) Mohan, V.; Lau, K.; Hui, D.; Bhattacharyya, D. Graphene-based materials and their composites: a review on production, applications and product limitations. *Composites, Part B* **2018**, *142*, 200−220.
(16) Zhao, S.; Yan, Y.; Gao, A.; Zhao, S.; Cui, J.; Zhang, G. Flexible Polydimethylsilane Nanocomposites Enhanced with a Three-Dimensional Graphene/Carbon Nanotube Bicontinuous Framework for High-Performance Electromagnetic Interference Shielding. *ACS Appl. Mater. Interfaces* **2018**, *10* (31), 26723−26732.
(17) Xin, G.; Zhu, W.; Deng, Y.; Cheng, J.; Zhang, L.; Chung, A.; De, S.; Lian, J. Microfluidics-enabled orientation and microstructure control of macroscopic graphene fibres. *Nat. Nanotechnol.* **2019**, *14* (2), 168−175.
(18) Xu, Z.; Liu, Y.; Zhao, X.; Peng, L.; Sun, H.; Xu, Y.; Ren, X.; Jin, C.; Xu, P.; Wang, M.; Gao, C. Ultrastiff and Strong Graphene Fibers via Full-Scale Synergetic Defect Engineering. *Adv. Mater.* **2016**, *28*, 6449−6456.
(19) Liu, Y.; Xu, Z.; Zhan, J.; Li, P.; Gao, C. Superb Electrically Conductive Graphene Fibers via Doping Strategy. *Adv. Mater.* **2016**, *28*, 7941−7947.
(20) Xin, G.; Yao, T.; Sun, H.; Scott, S.; Shao, D.; Wang, G.; Lian, J. Highly thermally conductive and mechanically strong graphene fibers. *Science* **2015**, *349*, 1083−1087.
(21) Jung, J.; Lee, H.; Ha, I.; Cho, H.; Kim, K.; Kwon, J.; Won, P.; Hong, S.; Ko, S. Highly Stretchable and Transparent Electromagnetic Interference Shielding Film Based on Silver Nanowire Percolation Network for Wearable Electronics Applications. *ACS Appl. Mater. Interfaces* **2017**, *9* (51), 44609−44616.
(22) Guo, L.; DeWeerth, S. High-density stretchable electronics: toward an integrated multilayer composite. *Adv. Mater.* **2010**, *22* (36), 4030−4033.
(23) Morent, R.; Geyter, N.; Axisa, F.; Smet, N.; Gengembre, L.; Leersnyder, E.; Leys, C.; Vanfleteren, J.; Rymarczyk, M.; Schacht, E.; Payen, E. Adhesion enhancement by a dielectric barrier discharge of PDMS used for flexible and stretchable electronics. *J. Phys. D: Appl. Phys.* **2007**, *40* (23), 7392−7401.
(24) Zhang, Y.; Weng, W.; Yang, J.; Liang, Y.; Yang, L.; Luo, X.; Zuo, W.; Zhu, M. Lithium-ion battery fiber constructed by diverse-dimensional carbon nanomaterials. *J. Mater. Sci.* **2019**, *54* (1), 582−591.
(25) Shen, J.; Hu, Y.; Shi, M.; Lu, X.; Qin, C.; Li, C.; Ye, M. Fast and facile preparation of graphene oxide and reduced graphene oxide nanoplatelets. *Chem. Mater.* **2009**, *21* (15), 3514−3520.
(26) Fang, B.; Xi, J.; Liu, Y.; Guo, F.; Xu, Z.; Gao, W.; Guo, D.; Li, P.; Gao, C. Wrinkle-stabilized metal-graphene hybrid fibers with zero temperature coefficient of resistance. *Nanoscale* **2017**, *9* (33), 12178−12188.
(27) Wang, Y.; Wang, Y.; Chen, J. J.; Guo, H.; Liang, K.; Marcus, K.; Peng, Q.; Zhang, J.; Feng, Z. A facile process combined with inkjet printing, surface modification and electroless deposition to fabricate adhesion-enhanced copper patterns on flexible polymer substrates for functional flexible electronics. *Electrochim. Acta* **2016**, *218*, 24−31.
(28) Wen, Y.; Huang, W.; Wang, B. A novel method for the preparation of Cu/Al2O3 nanocomposite. *Appl. Surf. Sci.* **2012**, *258* (7), 2935−2938.
(29) Wang, Y.; Lyu, S.; Luo, J.; Luo, Z.; Fu, Y.; Heng, Y.; Zhang, J.; Mo, D. Copper vertical micro dendrite fin arrays and their superior boiling heat transfer capability. *Appl. Surf. Sci.* **2017**, *422*, 388−393.
(30) Xu, Z.; Peng, L.; Liu, Y.; Liu, Z.; Sun, H.; Gao, W.; Gao, C. Experimental Guidance to Graphene Macroscopic Wet-Spun Fibers, Continuous Papers, and Ultralightweight Aerogels. *Chem. Mater.* **2017**, *29* (1), 319−330.
(31) Xin, G.; Sun, H.; Hu, T.; Fard, H.; Sun, X.; Koratkar, N.; Borca-Tasciuc, T.; Lian, J. Large-Area Freestanding Graphene Paper for Superior Thermal Management. *Adv. Mater.* **2014**, *26* (26), 4521−4526.
(32) Li, Z.; Xu, Z.; Liu, Y.; Wang, R.; Gao, C. Multifunctional non-woven fabrics of interfused graphene fibres. *Nat. Commun.* **2016**, *7* (1), 1−11.
(33) Zhang, Y.; Ren, Y.; Guo, H.; Bai, S. Enhanced thermal properties of PDMS composites containing vertically aligned graphene tubes. *Appl. Therm. Eng.* **2019**, *150*, 840−848.
(34) Fang, H.; Bai, S.; Wong, C. Microstructure engineering of graphene towards highly thermal conductive composites. *Composites, Part A* **2018**, *112*, 216−238.
(35) Rosen, B. Tensile failure of fibrous composites. *AIAA J.* **1964**, *2*, 1985−1991.
(36) Zweben, C. Tensile failure of fiber composites. *AIAA J.* **1968**, *6*, 2325−2331.
(37) Sano, Y.; Matsuzaki, R.; Ueda, M.; Todoroki, A.; Hirano, Y. 3D printing of discontinuous and continuous fibre composites using stereolithography. *Addit. Manuf.* **2018**, *24*, 521−527.
(38) Wang, G.; Liao, X.; Yang, J.; Tang, W.; Zhang, Y.; Jiang, Q.; Li, G. Frequency-selective and tunable electromagnetic shielding effectiveness via the sandwich structure of silicone rubber/graphene composite. *Compos. Sci. Technol.* **2019**, *184*, 107847−107854.
(39) Lin, S.; Wang, H.; Wu, F.; Wang, Q.; Bai, X.; Zu, D.; Song, J.; Wang, D.; Liu, Z.; Li, Z.; Tao, N.; Huang, K.; Lei, M.; Li, B.; Hui, W. Room-temperature production of silver-nanofiber film for large-area, transparent and flexible surface electromagnetic interference shielding. *npj Flex. Electron.* **2019**, *3* (1), 1−8.
(40) Liu, L.; Chen, W.; Zhang, H.; Wang, Q.; Guan, F.; Yu, Z. Flexible and Multifunctional Silk Textiles with Biomimetic Leaf-Like MXene/Silver Nanowire Nanostructures for Electromagnetic Interference Shielding, Humidity Monitoring, and Self-Derived Hydrophobicity. *Adv. Funct. Mater.* **2019**, *29* (44), 1905197.
(41) Ravindren, R.; Mondal, S.; Nath, K.; Das, N. Prediction of electrical conductivity, double percolation limit and electromagnetic interference shielding effectiveness of copper nanowire filled flexible polymer blend nanocomposites. *Composites, Part B* **2019**, *164*, 559−569.
(42) Yu, C.; Liang, X.; Zhao, T.; Zhu, P.; Li, G.; Cao, R.; Rong, S.; Wong, C. Synthesis and electromagnetic shielding performance of nickel nanowires with controllable morphology. *Mater. Lett.* **2019**, *236*, 112−115.
(43) Danlée, Y.; Bailly, C.; Huynen, I.; Piraux, L. Flexible Multilayer Combining Nickel Nanowires and Polymer Films for Broadband Microwave Absorption. *IEEE Trans. Electromagn. Compat.* **2019**, 1.
(44) Ryu, S.; Kim, J.; Cho, C.; Kim, W. Improvements of the Electrical Conductivity and EMI Shielding Efficiency for the Polycarbonate/ABS/Carbon Fiber Composites Prepared by Pultrusion Process. *Macromol. Res.* **2020**, *28* (2), 118−125.

https://dx.doi.org/10.1021/acsanm.0c00843
ACS Appl. Nano Mater. XXXX, XXX, XXX−XXX

(45) Chung, D.; Eddib, A. Effect of fiber lay-up configuration on the electromagnetic interference shielding effectiveness of continuous carbon fiber polymer-matrix composite. *Carbon* **2019**, *141*, 685−691.
(46) Tang, W.; Lu, L.; Xing, D.; Fang, H.; Liu, Q.; Teh, K. A carbon-fabric/polycarbonate sandwiched film with high tensile and EMI shielding comprehensive properties: an experimental study. *Composites, Part B* **2018**, *152*, 8−16.
(47) Shajari, S.; Arjmand, M.; Pawar, S.; Sundararaj, U.; Sudak, L. Synergistic effect of hybrid stainless steel fiber and carbon nanotube on mechanical properties and electromagnetic interference shielding of polypropylene nanocomposites. *Composites, Part B* **2019**, *165*, 662−670.
(48) Ameli, A.; Nofar, M.; Wang, S.; Park, C. Lightweight polypropylene/stainless-steel fiber composite foams with low percolation for efficient electromagnetic interference shielding. *ACS Appl. Mater. Interfaces* **2014**, *6* (14), 11091−11100.
(49) Lin, S.; Liu, J.; Wang, Q.; Zu, D.; Wang, H.; Wu, F.; Bai, X.; Song, J.; Liu, Z.; Li, Z.; Huang, K.; Li, B.; Lei, M.; Wu, H. Highly Robust, Flexible, and Large-Scale 3D-Metallized Sponge for High-Performance Electromagnetic Interference Shielding. *Adv. Mater. Technol.* **2020**, *5* (2), 1900761.
(50) Zhan, Y.; Oliviero, M.; Wang, J.; Sorrentino, A.; Buonocore, G.; Sorrentino, L.; Lavorgna, M.; Xia, H.; Iannace, S. Enhancing the EMI shielding of natural rubber-based supercritical CO_2 foams by exploiting their porous morphology and CNT segregated networks. *Nanoscale* **2019**, *11* (3), 1011−1020.
(51) Lu, D.; Mo, Z.; Liang, B.; Yang, L.; He, Z.; Zhu, H.; Tang, T.; Gui, X. Flexible, lightweight carbon nanotube sponges and composites for high-performance electromagnetic interference shielding. *Carbon* **2018**, *133*, 457−463.
(52) Chen, Y.; Zhang, H.; Yang, Y.; Wang, M.; Cao, A.; Yu, Z. High-performance epoxy nanocomposites reinforced with three-dimensional carbon nanotube sponge for electromagnetic interference shielding. *Adv. Funct. Mater.* **2016**, *26* (3), 447−455.
(53) Wu, Y.; Wang, Z.; Liu, X.; Shen, X.; Zheng, Q.; Xue, Q.; Kim, J. Ultralight graphene foam/conductive polymer composites for exceptional electromagnetic interference shielding. *ACS Appl. Mater. Interfaces* **2017**, *9* (10), 9059−9069.
(54) Wang, L.; Wu, Y.; Wang, Y.; Li, H.; Jiang, N.; Niu, K. Laterally Compressed Graphene Foam/Acrylonitrile Butadiene Styrene Composites for Electromagnetic Interference Shielding. *Composites, Part A* **2020**, *133*, 105887.
(55) Chen, Y.; Pötschke, P.; Pionteck, J.; Voit, B.; Qi, H. Multifunctional Cellulose/rGO/Fe_3O_4 Composite Aerogels for Electromagnetic Interference Shielding. *ACS Appl. Mater. Interfaces* **2020**, *12*, 22088.
(56) Zhang, D.; Liu, T.; Shu, J.; Liang, S.; Wang, X.; Cheng, J.; Wang, H.; Cao, M. Self-Assembly Construction of WS2−rGO Architecture with Green EMI Shielding. *ACS Appl. Mater. Interfaces* **2019**, *11* (30), 26807−26816.
(57) Sawai, P.; Chattopadhaya, P.; Banerjee, S. Synthesized reduce Graphene Oxide (rGO) filled Polyetherimide based nanocomposites for EMI Shielding applications. *Mater. Today Proc.* **2018**, *5* (3), 9989−9999.
(58) Yu, K.; Zeng, Y.; Wang, G.; Luo, X.; Li, T.; Zhao, J.; Qian, K.; Park, C. rGO/Fe_3O_4 hybrid induced ultra-efficient EMI shielding performance of phenolic-based carbon foam. *RSC Adv.* **2019**, *9* (36), 20643−20651.
(59) Chen, Z.; Xu, C.; Ma, C.; Ren, W.; Cheng, H. Lightweight and flexible graphene foam composites for high-performance electromagnetic interference shielding. *Adv. Mater.* **2013**, *25* (9), 1296−1300.
(60) Shahzad, F.; Kumar, P.; Kim, Y.; Hong, S.; Koo, C. Biomass-Derived Thermally Annealed Interconnected Sulfur-Doped Graphene as a Shield against Electromagnetic Interference. *ACS Appl. Mater. Interfaces* **2016**, *8* (14), 9361−9369.
(61) Shakir, M.; Khan, A.; Khan, R.; Javed, S.; Tariq, A.; Azeem, M.; Riaz, A.; Shafqat, A.; Cheema, H.; Akram, M.; Ahmad, I.; Jan, R. EMI shielding properties of polymer blends with inclusion of graphene nano platelets. *Results Phys.* **2019**, *14*, 102365−102372.
(62) Gupta, S.; Chang, C.; Anbalagan, A.; Lee, C.; Tai, N. Reduced graphene oxide/zinc oxide coated wearable electrically conductive cotton textile for high microwave absorption. *Compos. Sci. Technol.* **2020**, *188*, 107994−108002.
(63) Xu, Z.; Sun, H.; Zhao, X.; Gao, C. Ultrastrong fibers assembled from giant graphene oxide sheets. *Adv. Mater.* **2013**, *25* (2), 188−193.
(64) Manu, R.; Jayakrishnan, S. Influence of polymer additive molecular weight on surface and microstructural characteristics of electrodeposited copper. *Bull. Mater. Sci.* **2011**, *34* (2), 347−356.
(65) Parveen, S.; Arora, M. Microwave Absorption and EMI Shielding Behavior of Nanocomposites Based on Intrinsically Conducting Polymers, Graphene and Carbon Nanotubes. In *New Polymers for Special Applications*; Gomes, A., Eds.; IntechOpen: London, 2012; pp 73−112.
(66) Zhang, X.; Zhang, X.; Yang, M.; Yang, S.; Wu, H.; Guo, S.; Wang, Y. Ordered multilayer film of (graphene oxide/polymer and boron nitride/polymer) nanocomposites: An ideal EMI shielding material with excellent electrical insulation and high thermal conductivity. *Compos. Sci. Technol.* **2016**, *136*, 104−110.
(67) Song, W.; Cao, M.; Lu, M.; Bi, S.; Wang, C.; Liu, J.; Yuan, J.; Fan, L. Flexible graphene/polymer composite films in sandwich structures for effective electromagnetic interference shielding. *Carbon* **2014**, *66*, 67−76.
(68) Saini, P.; Choudhary, V.; Singh, B.; Mathur, R.; Dhawan, S. Enhanced microwave absorption behavior of polyaniline-CNT/polystyrene blend in 12.4−18.0 GHz range. *Synth. Met.* **2011**, *161* (15−16), 1522−1526.

https://dx.doi.org/10.1021/acsanm.0c00843
ACS Appl. Nano Mater. XXXX, XXX, XXX−XXX